J. Plasma Phys. (2021), *vol.* 87, 905870415

Published by Cambridge University Press
doi:10.1017/S0022377821000854

Counter differential rigid-rotation equilibrium of electrically non-neutral two-fluid plasma with finite pressure

Y. Nakajima [1],†, H. Himura [1],† and A. Sanpei [1]

[1] Department of Electronics, Kyoto Institute of Technology, Matsugasaki, Sakyo Ward, Kyoto 606-8585, Japan

(Received 6 June 2021; revised 9 August 2021; accepted 11 August 2021)

We derive the two-dimensional counter-differential rotation equilibria of two-component plasmas, composed of both ion and electron (e^-) clouds with finite temperatures, for the first time. In the equilibrium found in this study, as the density of the e^- cloud is always larger than that of the ion cloud, the entire system is a type of non-neutral plasma. Consequently, a bell-shaped negative potential well is formed in the two-component plasma. The self-electric field is also non-uniform along the r-axis. Moreover, the radii of the ion and e^- plasmas are different. Nonetheless, the pure ion as well as e^- plasmas exhibit corresponding rigid rotations around the plasma axis with different fluid velocities, as in a two-fluid plasma. Furthermore, the e^- plasma rotates in the same direction as that of $\boldsymbol{E} \times \boldsymbol{B}$, whereas the ion plasma counter-rotates overall. This counter-rotation is attributed to the contribution of the diamagnetic drift of the ion plasma because of its finite pressure.

Key words: strongly coupled plasmas, plasma dynamics, plasma confinement

1. Introduction

In modern plasma physics research, the two-fluid plasma model (Shumlak *et al.* 2011) is popular for analysing phenomena for which conventional hydrodynamic models, for example single-fluid equations and magnetohydrodynamics (generally abbreviated as MHD), are unsuitable. The two-fluid plasma equations permit a high degree of freedom in determining not only the spatiotemporal evolutions (Zhu, Francisquez & Rogers 2017; Morel *et al.* 2021) but also the equilibrium profiles (Ishida, Steinhauer & Peng 2010; Kanki & Nagata 2019; Ito & Nakajima 2021) of the density n_σ, pressure p_σ and mean velocity $\boldsymbol{v}_\sigma$ of the ion and electron fluids (hereafter, called plasma); subscript σ denotes either i or e because the equations comprise two sets of Euler equations as well as Maxwell's equations. However, a fundamental question arises on the assumption (De Jonghe & Keppens 2020; Mironov 2021; Zhang *et al.* 2021) that the ion and electron plasmas are electrically neutral, although it is not required by the two-fluid plasma model.

Non-neutral plasma physics (Kabantsev *et al.* 2014; Danielson *et al.* 2015) provides a novel insight into this question. Non-neutral plasmas are defined as exotic plasmas because

† Email addresses for correspondence: m0621027@edu.kit.ac.jp, himura@kit.ac.jp

they originally include only one charged particle species, for example either pure electrons (e^-) or pure ions (i^+). Such non-neutral plasmas have been extensively investigated (Kabantsev *et al.* 2001; Romé *et al.* 2019; Espinoza-Lozano, Calderón & Velazquez 2020) following the experimental verification of their robust rotation equilibrium (Davidson *et al.* 1991) with the confinement of the pure e^- plasma in a linear trap (Malmberg & Driscoll 1980). Pure i^+ plasmas (Dimonte 1981; Bollinger, Wineland & Dubin 1994; Dubin 2020; Viray, Miller & Raithel 2020) have also been studied. Several techniques developed in such experiments have been applied to produce antimatter, and CPT (charge, parity, and time reversal symmetry) sensitivity tests have been performed recently (Higaki *et al.* 2017; Fajans & Surko 2020). Moreover, toroidal e^- plasmas confined to magnetic surfaces without an externally applied electric field have been investigated (Berkery *et al.* 2007; Himura *et al.* 2010; Yoshida *et al.* 2012; Khamaru, Ganesh & Sengupta 2021), and magnetized electron–positron plasmas are being developed (Gilbert *et al.* 2001; Stoneking *et al.* 2020). In most recent studies, both i^+ and e^- plasmas have been used simultaneously as seed plasmas to explore the unverified physics of the equilibrium and stability of two-fluid plasmas in which n_i is never equal to n_e (Himura 2016; Akaike & Himura 2018, 2019; Yamada *et al.* 2018; Kato *et al.* 2019).

A two-fluid plasma with $n_i \neq n_e$ inherently results in a self-electric potential ϕ_s. Therefore, if the plasma is magnetically confined, it is not static but dynamic. The two-fluid plasma needs to keep rotating if it is in equilibrium. Davidson (Davidson 2001) derived a two-dimensional (2-D) differential rotation equilibrium under the assumption that the i^+ and e^- plasmas constituting the two-component plasma had zero temperature ($T_i = T_e = 0$ eV), and were cylindrically confined by a linear trap in a uniform axial magnetic field B_z, where B_z was assumed to be considerably larger than the self-magnetic field of the i^+ and e^- plasmas (Davidson 2001). In this case, the i^+ and e^- plasmas are independently rigid-rotated in the same direction but with different angular velocities ω_{ri} and ω_{re}, respectively, which is unlike the differential rotation observed in the Sun (Balbus *et al.* 2009). In modern terms, the differential rotation equilibrium of the i^+ and e^- plasmas can be described as a two-fluid plasma (Davidson & Uhm 1978) because $\boldsymbol{v}_i$ and $\boldsymbol{v}_e$ are different. The solutions for ω_{ri} and ω_{re} for the cold plasma case are expressed as $\omega_{ri}^{\pm} = -(\omega_{ci}/2)\{1 \pm (1 - 2\omega_{pi}^2(1 - 1/f)/\omega_{ci}^2)^{1/2}\}$ and $\omega_{re}^{\pm} = (\omega_{ce}/2)\{1 \pm (1 - 2\omega_{pe}^2(1 - f)/\omega_{ce}^2)^{1/2}\}$, where $\omega_{p\sigma}$ and $\omega_{c\sigma}$ are the plasma and cyclotron frequencies of the i^+ and e^- plasmas, respectively. Here, f is used as an indicator of the degree of non-neutrality of the two-component plasma: $f \equiv n_{i0}/n_{e0}$, where n_{i0} and n_{e0} are the densities of the i^+ and e^- plasmas, respectively. However, to the best of our knowledge, the 2-D differential rotation equilibrium of a two-fluid plasma with finite temperature has not yet been derived. In the case of finite temperature, diamagnetic drift because of the pressure gradient (Bellan 2008), whose direction depends on the polarity of the charge of the plasma species, unlike the $\boldsymbol{E} \times \boldsymbol{B}$ drift, occurs in two-fluid plasmas. In this study, we theoretically show that the 2-D differential rotation equilibrium continues to exist even in a two-fluid plasma with finite temperature, for the first time. Similar to the case of a single-component plasma with finite temperature (Davidson & Krall 1969), $n_i(r)$ and $n_e(r)$ develop corresponding bell-shaped profiles at rotational equilibrium. In addition, the plasma radii r_σ of the i^+ and e^- plasmas do not coincide but are different. Consequently, the radial component (E_r) of $-\nabla\phi_s$ increases nonlinearly. Nevertheless, both i^+ and e^- plasmas continue to exhibit corresponding rigid rotations. More notably, unlike the cold plasma case, the i^+ plasma counter-rotates around the plasma axis in the opposite direction of the e^- plasma, which rotates in the direction of $-\nabla\phi_s \times \boldsymbol{B}$ for the case where $f < 1$, i.e. $n_{i0} < n_{e0}$.

This counter-differential rotation equilibrium is attributed to the contribution of the diamagnetic drift of the i^+ plasma (Bellan 2008).

2. Derivation of the counter-differential rotation equilibria

Figure 1 depicts a solution of the counter-differential rotation equilibria. An infinitely long lithium-ion (Li^+) plasma column contains an infinitely long e^- plasma confined radially through $\boldsymbol{B}_z = B_0\hat{z}$, where $\hat{z}$ is the unit vector. The origin of the cylindrical coordinate system (r, θ, z) is located at the midplane of the coaxial plasmas, and the z-axis is selected to be parallel to $\boldsymbol{B}_z$. Both Li^+ and e^- plasmas have corresponding thermal equilibria and finite pressure $p_\sigma(r)$. The fluid velocity $\boldsymbol{v}_\sigma$ is assumed to be non-relativistic. Moreover, the plasma current $e(n_i\boldsymbol{v}_i - n_e\boldsymbol{v}_e)$ is insufficient to change B_z because of the low n_i and n_e. One of the possible states likely to exist is the rigid-rotation equilibrium of the two-fluid plasma in which both pure Li^+ and e^- plasmas can be independently relaxed into their corresponding thermal equilibria. Thus, the $\omega_{r\sigma}$ values are constant. In this case, the counter differential rotation equilibrium can be derived as follows.

Because each plasma rotates as a rigid body around the z-axis, the θ component of $\boldsymbol{v}_\sigma$ ($v_{\theta\sigma}$) is proportional to r and therefore, $v_{\sigma\theta} = \omega_{r\sigma} r$. The term ∇p_σ is equivalent to $k_B T_\sigma \nabla n_\sigma$ because T_σ is spatially uniform at thermal equilibrium. Hence, the equation of steady-state motion for both plasmas can be expressed as $m_\sigma n_\sigma(\boldsymbol{v}_\sigma \cdot \nabla)\boldsymbol{v}_\sigma = n_\sigma q_\sigma(\boldsymbol{v}_\sigma \times \boldsymbol{B}_z - \nabla\phi_s) - k_B T_\sigma \nabla n_\sigma$, where m_σ and q_σ represent the mass number and elementary charge of each species, respectively. Solving this equation for $n_\sigma(r)$,

$$n_\sigma(r) = n_{\sigma 0} \exp\left(-\frac{\psi_\sigma}{k_B T_\sigma}\right), \quad (\sigma = i, e), \tag{2.1}$$

where

$$\psi_\sigma(r) \equiv q_\sigma\phi_s(r) - \tfrac{1}{2} m_\sigma r^2(\mathrm{sgn}(q_\sigma)\omega_{c\sigma}\omega_{r\sigma} + \omega_{r\sigma}^2). \tag{2.2}$$

The coefficient $n_{\sigma 0}$ on the right-hand side of (2.1) represents the value of n_σ on the z-axis, where $r = 0$. In addition, ψ_σ are the corresponding effective potential energies (Davidson 2001) of the singly ionized ions and e^- plasmas. Substituting them in Poisson's equation, the rotation equilibrium equation with finite T_σ can be expressed as

$$\frac{1}{r}\frac{\mathrm{d}}{\mathrm{d}r}\left(r\frac{\mathrm{d}}{\mathrm{d}r}\phi_s\right) = \sum_{\sigma=i,e} -\frac{q_\sigma}{\epsilon_0} n_{\sigma 0} \exp\left(-\frac{\psi_\sigma}{k_B T_\sigma}\right). \tag{2.3}$$

To numerically determine the solutions of (2.3), we apply the measured values in the beam experiment upgrade (BX-U) linear trap experiments (Himura 2016; Akaike & Himura 2018, 2019; Yamada *et al.* 2018; Kato *et al.* 2019), as examples for the calculation. The boundary condition of ϕ_s is the same as that of the BX-U as well, as listed in table 1. Although the value of B_0 is variable, it is fixed to 0.13 T in the presented calculation. Lithium (Li^+) is employed as the singly ionized ion. The value of n_{i0} can be varied in the 10^{11}–10^{12} m^{-3} range, whereas n_{e0} is in the 10^{12}–10^{13} m^{-3} range. For T_σ, we assume $T_i = T_e = 2$ eV because the confinement time is considerably greater than the binary collision time. This observation implies two-fluid rotational equilibrium. To determine solutions within the n_i and n_e ranges in table 1, the coefficients of n_{i0} and n_{e0} are set to 1×10^{11} and 5×10^{12} m^{-3}, respectively. Thus, $n_{i0}/n_{e0} = 0.02$. Under these conditions, the Gauss–Seidel method was employed to solve (2.3). Values of ω_{ri} and ω_{re} are also computational parameters. First, we obtain $\phi_s(r)$ from (2.2) and (2.3) by substituting independent values into ω_{ri} and ω_{re} one by one. Then, the obtained $\phi_s(r)$ is utilized

https://doi.org/10.1017/S0022377821000854 Published online by Cambridge University Press

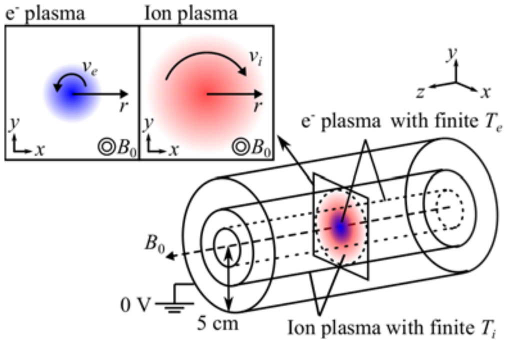

FIGURE 1. Illustration of the differential rigid-rotation equilibrium of a two-component (two-fluid) plasma model with finite T_σ. To find solutions in the realistic case of laboratory plasmas, we refer to the beam experiment upgrade (BX-U) linear trap experiment (Himura 2016; Akaike & Himura 2018, 2019; Yamada *et al.* 2018; Kato *et al.* 2019), where Li^+ and e^- plasmas constitute the two-component plasma.

Axial magnetic field	B_z	$\leq$0.13 T
Vacuum pressure	p_0	$(5-10) \times 10^{-10}$ Torr
Pure ion plasma	Mass of Li^+ ion	6.941 u
	Anode temperature	$\approx$1300 K
	Acceleration voltage	$>$3 V
	n_i	10^{10} - 10^{12} m^{-3}
Pure e^- plasma	Cathode temperature	$\approx$1300 K
	Acceleration voltage	5–15 V
	n_e	10^{11}–10^{13} m^{-3}
Confinement time	Pure e^- plasma	$>$18 s
	Pure ion plasma	$\sim$1–10 s
	Two-fluid plasma	10 µs $-$ 1 s
Collision time[a]	$e^- - e^-$	0.1–0.9 ms
	ion - ion	0.1–1.3 s
	e^- - ion	0.1–0.9 ms
	ion - e^-	0.15–1.4 s
Ion skin depth		$>10^2$ m
Boundary condition:	$\phi_s = 0$ V at $r = 5$ cm	

[a]All the collision times are calculated using the values of n_i and n_e listed above.

TABLE 1. Nominal parameters of the BX-U machine and assumed boundary condition for ϕ_s in this calculation.

to calculate the corresponding $n_\sigma(r)$ from (2.1). Using these numerical schemes, we systematically find self-consistent sets of solutions of ψ_s, n_i and n_e that satisfy (2.1)–(2.3) simultaneously even with finite T_i and T_e, as shown below.

3. Possible ω_{re} and ω_{ri} with which counter-differential rigid-rotation equilibria exist

Figure 2 shows the dependency of $\omega_{r\sigma}$ on n_{i0}/n_{e0}, where $\omega_{r\sigma}$ is normalized by the cyclotron frequency $\omega_{c\sigma}$. For the three cases where $n_{i0}/n_{e0} = 0.02$, 0.5 and 0.9, the possible ranges of ω_{re} and ω_{ri} in which rigid-rotation equilibria of the two-fluid plasma exist are denoted by the six solid-line sections, where the red and blue colours represent

https://doi.org/10.1017/S0022377821000854 Published online by Cambridge University Press

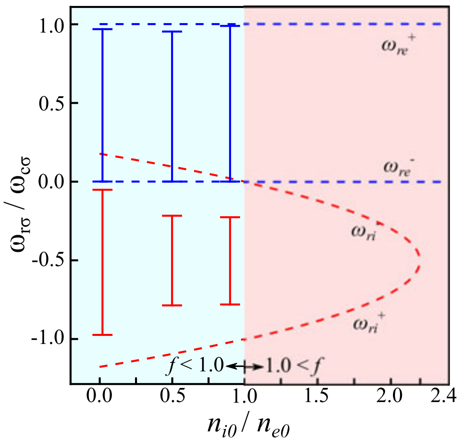

FIGURE 2. Dependency of $\omega_{r\sigma}$ on n_{i0}/n_{e0}. Here $\omega_{r\sigma}$ is normalized by the corresponding cyclotron frequency $\omega_{c\sigma}$. The dashed (red) curve shows the possible solutions (ω_{ri}^{+} and ω_{ri}^{-}) for a two-component plasma with $T_i = T_e = 0$ eV, whereas the dashed (blue) lines indicate the possible solutions (ω_{re}^{+} and ω_{re}^{-}) for a two-component plasma with $T_i = T_e = 0$. $T_e = 0$ eV. The values of n_{e0} are set to 5×10^{12} m^{-3}. As can be observed, for a two-component plasma with finite T_σ, the possible ranges of ω_σ are limited. These are denoted by the corresponding solid-line sections, where the blue colour represents e^- plasma and the red represents Li$^+$ plasma.

ω_{re} and ω_{ri}, respectively.[1] For the reader's understanding, it should be noted that the value of $\omega_{r\sigma}$ of a single-component plasma such as pure e^- plasma must be either $\omega_{r\sigma}^{+}$ (fast mode) or $\omega_{r\sigma}^{-}$ (slow mode) if T_σ is zero. For $T_\sigma \neq 0$, $\omega_{r\sigma}$ of a single-component plasma can take any value between $\omega_{r\sigma}^{+}$ and $\omega_{r\sigma}^{-}$. However, for two-fluid plasmas with finite T_σ, the possible ranges of both ω_{re} and ω_{ri} are limited. This is noticeable for ω_{ri}, as depicted in figure 2. The sign of ω_{re} is always positive. On the other hand, the sign of ω_{ri} is always negative, contrary to the case of one-component pure ion plasmas. The different signs of ω_{re} and ω_{ri} physically imply that the Li$^+$ and e^- plasmas rigid-rotate in opposite directions. As previously mentioned, B_z is along the positive direction of the z-axis, whereas $E_r(= -\nabla_r\phi_s)$ is from the plasma edge toward the plasma axis, inward. This can be deduced from the fact that $n_{e0} > n_{i0}$. Overall, it is recognized that the e^- plasma rotates in the direction of $E_r \times B_z$, whereas the Li$^+$ plasma counter-rotates in the opposite direction of $E_r \times B_z$. Because $\omega_{ri} \neq \omega_{re}$, this can be considered as the counter-differential rotation equilibrium of two-fluid plasmas. As example solutions, we present extraordinary cases. When ω_{re}/ω_{ce} takes a minimum value of 1.6×10^{-4}, ω_{ri}/ω_{ci} can take any value in the $-0.97 < \omega_{ri}/\omega_{ci} < -0.05$ range. Such arbitrariness is provided by the fact that changes in the profiles of $n_\sigma(r)$ and $\phi_s(r)$ occur self-consistently to satisfy (2.1)–(2.3).

4. The finite temperature effect

The counter-rotation of Li$^+$ plasma at rigid-rotor equilibrium is attributed to the finite p_σ. Figure 3 shows the radial profiles of the azimuthal components of $\boldsymbol{E} \times \boldsymbol{B}$ ($\equiv v_\phi = (1/B_0)\,\mathrm{d}\phi_s/\mathrm{d}r$) and the diamagnetic ($\equiv v_{d\sigma} = -(k_B T_\sigma/n_\sigma q_\sigma B_0)\,\mathrm{d}n_\sigma/\mathrm{d}r$) drift terms along with v_σ. These are calculated from a typical set of equilibrium solutions of $\phi_s(r)$ and $n_\sigma(r)$, as depicted in figure 4. Figure 3 shows that the sign of v_ϕ is positive along the entire r-axis. However, $|v_\phi|$ is one order of magnitude smaller than the absolute value of

[1]If n_{e0} is smaller, the range of f where real solutions of $\omega_{ri}^{\pm}$ exist extends beyond $f \sim 2$, correspondingly. Finally, $n_i(0)$ approaches the Brillouin density of a pure ion plasma as f approaches infinity by decreasing n_{e0}.

https://doi.org/10.1017/S0022377821000854 Published online by Cambridge University Press

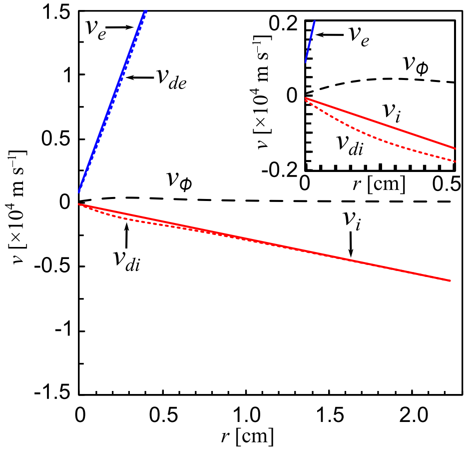

FIGURE 3. Radial profiles of the azimuthal components of v_ϕ (black dashed curves), $v_{d\sigma}$ (red dotted curves for Li^+ plasma and blue for e^- plasma) and v_σ (two solid red and blue lines) for a typical set of equilibrium solutions obtained for the case where $\omega_{ri} = -3.3 \times 10^5$ and $\omega_{re} = 3.6 \times 10^6$ rad s^{-1}. Both Li^+ and e^- exhibit counter-differential rigid-rotation equilibrium.

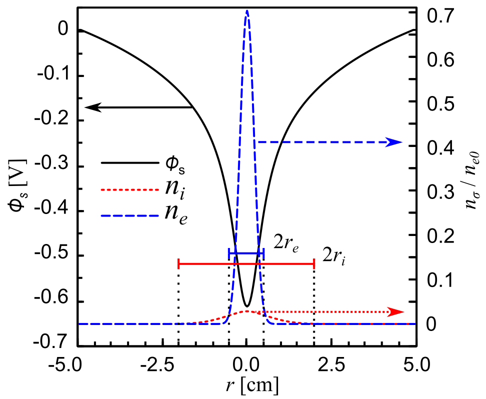

FIGURE 4. Radial profiles of $\phi_s(r)$ and $n_\sigma(r)$ for the set of equilibrium solutions shown in figure 3. Here r_i and r_e are never equal but are different when the two-component (two-fluid) plasma is in counter-differential rigid-rotation equilibrium. In addition, the lengths of r_i and r_e in the two-fluid equilibrium are smaller than those calculated for the pure Li^+ and e^- plasmas.

v_{di}, which is negative in the entire plasma, causing counter-rotation. Here, we note that v_ϕ and v_{di} change nonlinearly along the r-axis, which can be clearly recognized in the inset of figure 3. However, v_i, composed of v_ϕ and v_{di}, increases linearly along the r-axis, resulting in rigid-body rotation.

The same linearization occurs for v_e as well, as depicted in figure 3. Counter-differential rigid-rotation equilibrium is caused by the balance between p_σ and ϕ_s perpendicular to B_z, which is qualitatively similar to the study of non-uniform p_σ and ϕ_s on toroidal magnetic surfaces (Pedersen & Boozer 2002; Himura *et al.* 2007).

At counter-differential rotation equilibrium, $n_\sigma(r)$ assumes the corresponding bell-shaped profile, which is qualitatively the same as that in the cold plasma case. However, because of finite T_σ, the pressure-gradient terms ($k_B T_\sigma \nabla n_\sigma$) play dominant roles in maintaining the corresponding rotational equilibria, as mentioned above. In figure 4,

https://doi.org/10.1017/S0022377821000854 Published online by Cambridge University Press

the value of $n_i(0)$ is approximately 1.4×10^{11} m^{-3}, which is greater than n_{i0}, whereas $n_e(0) \approx 3.5 \times 10^{12}$ m^{-3} is smaller than n_{e0}. The difference between n_i and n_e indicates that the two-fluid plasma is electrically non-neutral. Because $n_i(0) < n_e(0)$, ϕ_s becomes negative at $r = 0$. However, in addition to the plasma axis, the negative ϕ_s extends over the entire plasma, regardless of n_i. The minimum value of ϕ_s is at $r = 0$, which is approximately -0.7 V in this case. The curvature of $\phi_s(r)$ becomes convex toward the top, as observable in figure 4.

For $n_\sigma(r)$, their maxima appear at the plasma centre ($r = 0$) and decrease monotonically, consistent with $\phi_s(r)$. However, the remarkable result inferred from the profiles of $n_i(r)$ and $n_e(r)$ is that r_i and r_e never become equal and always remain different. Defining r_σ as the distance between the plasma centre and the coordinate, where n_σ decreases to 1/10 of $n_\sigma(0)$ (i.e. $n_\sigma(r_\sigma)/n_\sigma(0) = 1/10$), r_i and r_e are approximately 2.5 and 0.5 cm, respectively, in the presented case.

The obtained bell-shaped profiles shown in figure 4 may be due to the finite-temperature effect (Davidson & Krall 1969) to some extent. However, the past study assumed that the Debye length λ was sufficiently short compared with the plasma radius r_p. This assumption implied that either n_e was relatively high or r_p was relatively long. Contrary to these, the present result is obtained from a different parameter regime in which n_σ is relatively lower and T_σ is finite. As a result, λ has the same order as that of r_p.

5. On the radii of single-component and two-fluid plasmas

The lengths of r_σ reduce when the pure ion as well as e^- plasmas with finite T_σ are in counter-differential rotation equilibrium together. Substituting the values of $n_\sigma(0)$ in figure 4 in Davidson's formula[2] derived for a single-component plasma, r_i and r_e are expected to be approximately 6 and 1 cm, respectively. Here, $r_\sigma \approx -\{\sqrt{k_B T_\sigma/m_\sigma}/\omega_{p\sigma}\} \ln[(2(\omega_{r\sigma}\omega_{c\sigma} - \omega_{r\sigma}^2)/\omega_{p\sigma}^2) - 1]$. This discrepancy is caused by the increase in ψ_i of the two-fluid plasma. When a single-component ion plasma is in rotational equilibrium, ϕ_s is estimated to be of the order of $er_i^2 n_{i0}/\epsilon_0$. In addition, n_{i0} must always be smaller than the Brillouin density (Davidson 2001) such that $\omega_{ri}^- \approx -\omega_{pi}^2/2\omega_{ci}$, in the case where $\omega_{ri}^- \ll \omega_{ci}$. Substituting these in (2.2), we estimate ψ_i^0 of the single-component ion plasma as

$$\psi_i^0 = e\phi_s - \frac{1}{2} m_i r^2 \{\omega_{ci}\omega_{ri}^- - (\omega_{ri}^-)^2\} \approx \frac{5}{4}\frac{e^2 n_{i0}}{\epsilon_0} r_i^2. \tag{5.1}$$

Here, we used the following relationship: $m_i r_i^2 \omega_{pi}^2 = e^2 r_i^2 n_{i0}/\epsilon_0$. However, in the case of a two-component plasma with $0 < n_{i0} < n_{e0}$, $\phi_s \approx e r_i^2 n_e(0)/\epsilon_0$ and $\omega_{ri}^- \approx (n_{e0}/n_{i0})\omega_{pi}^2/2\omega_{ci}$. Thus, for the counter-differential rotation equilibrium example shown in figures 3 and 4, $\omega_{ri} \approx -(n_{e0}/n_{i0})\omega_{pi}^2/2\omega_{ci}$ because $\omega_{ri} = -0.19 \times \omega_{ci} = -1.1 \times \omega_{ri}^-$. Therefore, ψ_i of the two-component plasma is derived as

$$\psi_i \approx \frac{5}{4}\frac{e^2 n_{e0}}{\epsilon_0} r_i^2 = \frac{n_{e0}}{n_{i0}} \psi_i^0 \quad (> \psi_i^0). \tag{5.2}$$

According to (2.1), an increase in ψ_i causes a rapid decrease in n_i as $|r|$ increases, resulting in a narrower $n_i(r)$ as seen in figure 4. In general, for $0 < n_{i0} < n_{e0}$, r_i of a two-component

[2]This formula was derived based on the assumption that the conductor wall was biased to make $\phi_s(0) = 0$ V and $n_\sigma(0) = n_{\sigma 0}$; however, the estimate can be applied when the conductor wall is grounded. In this case, $n_\sigma(0)$ is obtained using $n_{\sigma 0}\exp(-q_\sigma \phi_s(0)/k_B T_\sigma)$, and the magnitude of the $\exp(-q_\sigma \phi_s(0)/k_B T_\sigma)$ term is of the order of unity – therefore, $n_{\sigma 0} \approx n_\sigma(0)$.

https://doi.org/10.1017/S0022377821000854 Published online by Cambridge University Press

plasma becomes approximately $\sqrt{n_{i0}/n_{e0}}$ times smaller than that of a single-component ion plasma.

The shorter r_e is also explained by the increase in ψ_e. In the equilibrium depicted in figures 3 and 4, ω_{re}/ω_{ce} is $\sim 10^{-4}$, which is an order of magnitude greater than the slow mode: $\omega_{re}^{-}/\omega_{ce} \sim 10^{-5}$. In addition, $(1 - n_{i0}/n_{e0}) \approx 1$ in this case. Thus, ϕ_s is almost the same for the pure e^- as well as two-component plasma. We compare the two effective potentials of the two cases. The effective potential of the pure e^- plasma is ψ_e^0. Substituting these in (2.1) and (2.2), we estimate ψ_e and ψ_e^0 as

$$\psi_e \approx \frac{\omega_{re}}{\omega_{re}^{-}} \psi_e^0 > \psi_e^0. \tag{5.3}$$

Based on these considerations, it is concluded that the two-component plasma becomes narrower overall.

6. Summary

In summary, the 2-D rigid-rotation equilibria of electrically non-neutral two-component (two-fluid) plasma with finite T_σ were presented in this study, for the first time. Furthermore, self-consistent solutions of the differential rigid-rotation equilibria were determined. However, the possible range of ω_σ becomes narrower than that of the two-component plasma with $T_\sigma = 0$. Remarkably, in contrast to the cold plasma case, the ion plasma is only permitted to counter-rotate because of its diamagnetic drift. In the future, we intend to investigate the following. In this study, three cases of e^- rich plasmas ($n_{i0}/n_{e0} = 0.02$, 0.5, and 0.9) were presented to straightaway show the existence of counter differential rigid-rotation equilibria. A complete set of possible ranges of ω_σ for different values of n_{i0}/n_{e0} will be considered. Cases with $T_i \neq T_e$ will be investigated as well. Moreover, in the BX-U experiment, there is no constraint that the two-fluid plasma must rotate rigidly. A more general solution would be to use $\omega_i(r)$ and $\omega_e(r)$. In fact, the axial length of actual plasmas is finite so that three-dimensional computations are suitable for comparison between experiments and simulations.

Finally, in the case of a small fraction of positive ions in an otherwise pure electron plasma, the ion resonance instability has been observed to emerge not only theoretically (Levy, Daugherty & Buneman 1969) but also experimentally (Marksteiner *et al.* 2008). Therefore, a stability analysis would be required for the counter differential rigid-rotation equilibrium with a minimal value of f. Since $\lambda \approx r_\sigma$ in the presented parameter regime, collective plasma effects are not expected to be significant. Perhaps, such an instability might not grow as much.

Acknowledgements

The authors thank Mr T. Okada of the Kyoto Institute of Technology, Professor E.S. Okada of Osaka University and Dr M. Sengupta of Saskatchewan University for the discussions and comments. We would like to thank Editage (www.editage.com) for English language editing.

Editor Per Helander thanks the referees for their advice in evaluating this article.

Funding

This work is supported by JSPS KAKENHI (grant no. 20KK0063 and 21H01056) and the National Institute for Fusion Science (grant no. NIFS20KOAP035).

Declaration of interest

The authors report no conflict of interest.

REFERENCES

AKAIKE, K. & HIMURA, H. 2018 Studies of ion leakage from a penning trap induced by potential barrier closure. *Phys. Plasmas* **25** (12), 122108.

AKAIKE, K. & HIMURA, H. 2019 A method for avoiding following ion leakage from a penning trap. *Plasma Fusion Res*. **14**, 4401149–4401149.

BALBUS, S.A., BONART, J., LATTER, H.N. & WEISS, N.O. 2009 Differential rotation and convection in the Sun. *Mon. Not. R. Astron. Soc*. **400** (1), 176–182.

BELLAN, P.M. 2008 *Fundamentals of Plasma Physics*. Cambridge University Press.

BERKERY, J.W., PEDERSEN, T.S., KREMER, J.P., MARKSTEINER, Q.R., LEFRANCOIS, R.G., HAHN, M.S. & BRENNER, P.W. 2007 Confinement of pure electron plasmas in the Columbia non-neutral torus. *Phys. Plasmas* **14** (6), 062503.

BOLLINGER, J.J., WINELAND, D.J. & DUBIN, D.H. E. 1994 Non-neutral ion plasmas and crystals, laser cooling, and atomic clocks. *Phys. Plasmas* **1** (5), 1403–1414.

DANIELSON, J.R., DUBIN, D.H.E., GREAVES, R.G. & SURKO, C.M. 2015 Plasma and trap-based techniques for science with positrons. *Rev. Mod. Phys*. **87** (1), 247.

DAVIDSON, R.C. 2001 *Physics of Nonneutral Plasmas*. World Scientific Publishing Company.

DAVIDSON, R.C., CHAN, H.-W., CHEN, C. & LUND, S. 1991 Equilibrium and stability properties of intense non-neutral electron flow. *Rev. Mod. Phys*. **63** (2), 341.

DAVIDSON, R.C. & KRALL, N.A. 1969 Vlasov description of an electron gas in a magnetic field. *Phys. Rev. Lett*. **22** (16), 833.

DAVIDSON, R.C. & UHM, H.-S. 1978 Influence of finite ion larmor radius effects on the ion resonance instability in a nonneutral plasma column. *Phys. Fluids* **21** (1), 60–71.

DE JONGHE, J. & KEPPENS, R. 2020 A two-fluid analysis of waves in a warm ion–electron plasma. *Phys. Plasmas* **27** (12), 122107.

DIMONTE, G. 1981 Ion Langmuir waves in a nonneutral plasma. *Phys. Rev. Lett*. **46** (1), 26.

DUBIN, D.H.E. 2020 Normal modes, rotational inertia, and thermal fluctuations of trapped ion crystals. *Phys. Plasmas* **27** (10), 102107.

ESPINOZA-LOZANO, B.F.I., CALDERÓN, F.A. & VELAZQUEZ, L. 2020 A pure non-neutral plasma under an external harmonic field: equilibrium thermodynamics and chaos. *J. Stat. Mech. Theory Exp*. **2020** (4), 043205.

FAJANS, J. & SURKO, C.M. 2020 Plasma and trap-based techniques for science with antimatter. *Phys. Plasmas* **27** (3), 030601.

GILBERT, S.J., DUBIN, D.H.E., GREAVES, R.G. & SURKO, C.M. 2001 An electron–positron beam–plasma instability. *Phys. Plasmas* **8** (11), 4982–4994.

HIGAKI, H., KAGA, C., FUKUSHIMA, K., OKAMOTO, H., NAGATA, Y., KANAI, Y. & YAMAZAKI, Y. 2017 Simultaneous confinement of low-energy electrons and positrons in a compact magnetic mirror trap. *New J. Phys*. **19** (2), 023016.

HIMURA, H. 2016 BX-U linear trap for one-way production and confinement of Li+ and e- plasmas. *Nucl. Instrum. Meth. Phys. Res*. B **811**, 100–107.

HIMURA, H., NAKAMURA, K., MASAMUNE, S., ISOBE, M. & SHIMIZU, A. 2010 Outward electron orbit extending to inward part of closed helical magnetic surfaces surrounded by shifted negative space potential. *Phys. Plasmas* **17** (3), 032507.

HIMURA, H., WAKABAYASHI, H., YAMAMOTO, Y., ISOBE, M., OKAMURA, S., MATSUOKA, K., SANPEI, A. & MASAMUNE, S. 2007 Experimental verification of nonconstant potential and density on magnetic surfaces of helical nonneutral plasmas. *Phys. Plasmas* **14** (2), 022507.

ISHIDA, A., STEINHAUER, L.C. & PENG, Y.-K. M. 2010 Two-fluid low-collisionality equilibrium model and application to spherical torus plasmas. *Phys. Plasmas* **17** (12), 122507.

ITO, A. & NAKAJIMA, N. 2021 Two-fluid and finite Larmor radius effects on high-beta tokamak equilibria with flow in reduced magnetohydrodynamics. *Phys. Scr*. **96** (3), 035602.

KABANTSEV, A.A., CHIM, C.Y., O'NEIL, T.M. & DRISCOLL, C.F. 2014 Diocotron and Kelvin mode damping from a flux through the critical layer. *Phys. Rev. Lett*. **112** (11), 115003.

KABANTSEV, A.A., DRISCOLL, C.F., HILSABECK, T.J., O'NEIL, T.M. & YU, J.H. 2001 Trapped-particle asymmetry modes in single-species plasmas. *Phys. Rev. Lett*. **87** (22), 225002.

KANKI, T. & NAGATA, M. 2019 Computation of two-fluid flowing equilibrium of spherical torus plasma using multi-grid method. *Intl J. Appl. Electromagn. Mech*. **59** (2), 439–446.

KATO, T., HIMURA, H., SOWA, S. & SANPEI, A. 2019 Controlling the diameter of a pure electron plasma to produce an exact two-fluid plasma state in a nested trap. *Plasma Fusion Res*. **14**, 1201039–1201039.

KHAMARU, S., GANESH, R. & SENGUPTA, M. 2021 A novel quiescent quasi-steady state of a toroidal electron plasma. *Phys. Plasmas* **28** (4), 042101.

LEVY, R.H., DAUGHERTY, J.D. & BUNEMAN, O. 1969 Ion resonance instability in grossly nonneutral plasmas. *Phys. Fluids* **12** (12), 2616–2629.

MALMBERG, J.H. & DRISCOLL, C.F. 1980 Long-time containment of a pure electron plasma. *Phys. Rev. Lett*. **44** (10), 654.

MARKSTEINER, Q.R., PEDERSEN, T.S., BERKERY, J.W., HAHN, M.S., MENDEZ, J.M., DE GEVIGNEY, B.D. & HIMURA, H. 2008 Observations of an ion-driven instability in non-neutral plasmas confined on magnetic surfaces. *Phys. Rev. Lett*. **100** (6), 065002.

MIRONOV, V.L. 2021 Self-consistent hydrodynamic two-fluid model of vortex plasma. *Phys. Fluids* **33** (3), 037116.

MOREL, B., GIUST, R., ARDANEH, K. & COURVOISIER, F. 2021 A solver based on pseudo-spectral analytical time-domain method for the two-fluid plasma model. *Sci. Rep*. **11** (1), 1–10.

PEDERSEN, T.S. & BOOZER, A.H. 2002 Confinement of nonneutral plasmas on magnetic surfaces. *Phys. Rev. Lett*. **88** (20), 205002.

ROMÉ, M., MAERO, G., PANZERI, N. & POZZOLI, R. 2019 Selective excitation of Kelvin–Helmholtz modes with rotating electric fields. In *European Physical Society Conference on Plasma Physics*. European Physical Society.

SHUMLAK, U., LILLY, R., REDDELL, N., SOUSA, E. & SRINIVASAN, B. 2011 Advanced physics calculations using a multi-fluid plasma model. *Comput. Phys. Commun*. **182** (9), 1767–1770.

STONEKING, M.R., PEDERSEN, T.S., HELANDER, P., CHEN, H., HERGENHAHN, U., STENSON, E.V., FIKSEL, G., VON DER LINDEN, J., SAITOH, H., SURKO, C.M., *et al.* 2020 A new frontier in laboratory physics: magnetized electron–positron plasmas. *J. Plasma Phys*. **86** (6), 1–26.

VIRAY, M.A., MILLER, S.A. & RAITHEL, G. 2020 Coulomb expansion of a cold non-neutral rubidium plasma. *Phys. Rev.* A **102** (3), 033303.

YAMADA, S., HIMURA, H., KATO, T., OKADA, S., SANPEI, A. & MASAMUNE, S. 2018 Two-dimensional macroscopic shapes of lithium ion and electron plasmas after elapse of two-fluid plasma state. In *AIP Conference Proceedings*, vol. 1928, p. 020016. AIP Publishing LLC.

YOSHIDA, Z., SAITOH, H., YANO, Y., MIKAMI, H., KASAOKA, N., SAKAMOTO, W., MORIKAWA, J., FURUKAWA, M. & MAHAJAN, S.M. 2012 Self-organized confinement by magnetic dipole: recent results from RT-1 and theoretical modeling. *Plasma Phys. Control. Fusion* **55** (1), 014018.

ZHANG, F., POEDTS, S., LANI, A., KUŹMA, B. & MURAWSKI, K. 2021 Two-fluid modeling of acoustic wave propagation in gravitationally stratified isothermal media. *Astrophys. J*. **911** (2), 119.

ZHU, B., FRANCISQUEZ, M. & ROGERS, B.N. 2017 Global 3D two-fluid simulations of the tokamak edge region: turbulence, transport, profile evolution, and spontaneous $E \times B$ rotation. *Phys. Plasmas* **24** (5), 055903.